COMPUTATION OF INTERFACIAL AREAS, COMMON CURVE LENGTHS AND INTERFACIAL CURVATURES FROM EXPERIMENTALLY DERIVED DATA

JAMES E. MCCLURE[1], DAVID ADALSTEINSSON[2], DORTHE WILDENSCHILD[3], WILLIAM G. GRAY[1], AND CASS T. MILLER[1]

[1] Department of Environmental Sciences and Engineering, University of North Carolina, Chapel Hill, North Carolina 27599-7431, USA

[2] Department of Mathematics, University of North Carolina, Chapel Hill, North Carolina 27599-3250, USA

[3] Department of Geosciences, Department of Civil, Construction and Environmental Engineering, Oregon State University, Corvallis, Oregon 97311, USA

Abstract

Microscale investigation of porous medium systems contributes to our understanding of macroscopic systems at a fundamental level and can be used to formulate closed macroscale models. We present an overview of methods designed to obtain accurate estimates of interfacial areas, common curve lengths, and interfacial curvatures for porous medium data sets. We then describe how these methods can be applied to experimentally generated data and examine data sets obtained using computed micro-tomography (CMT) as an example. Discussion of pertinent issues is provided, including the nature of the raw data, sorts of experimental data that can be collected to minimize errors, the impact of smoothing operations applied to the raw data, and the resolution necessary to obtain reliable estimates of the variables of interest.

1. INTRODUCTION

Interfaces and common curves occur in multiphase porous medium systems. Understanding their extent and behavior is important for developing a mature understanding and rigorous models of these complex systems. Failure to properly account for the physics of interfaces and common curves is a suspected cause of shortcomings observed in traditional multiphase models [7]. Porous medium continuum-scale mathematical models that include these microscale surfaces and curves provide a means to account for their physical impact at the macroscale [6]. Methods that resolve microscale details, either experimentally or computationally, provide opportunities to study various aspects of these models. Obtaining approximations of interfaces and quantitative measures of their properties (e.g., extent measure, curvature) is desirable for

the study of a variety of phenomena, including mass transfer processes [9], viscous coupling [10], and hysteretic behavior of constitutive relationships linking capillary pressure, fluid saturations, and interfacial areas [1, 8, 13].

Computed micro-tomography (CMT) is a non-invasive technique that can be used to obtain a three-dimensional representation of experimental porous medium systems. CMT measures the attenuation of a high flux of photons applied to a porous media system. The data collected is can be used to reconstruct the system in the form of a highly resolved three-dimensional spatial field of attenuation characteristics and thereby provide an image of the structure of the medium and the distribution of the phases [15]. This approach has been applied to both air-water and oil-water porous medium systems, effectively resolving features at the micron scale [2]. The challenge, then, is to analyze the images to obtain quantitative measures of the features revealed in the images.

The marching cubes (MC) algorithm is sometimes used to approximate interfaces in multiphase porous medium systems. The MC algorithm was first developed to obtain surfaces of constant density from three-dimensional medical data. However, it can be used to approximate the location of any surface defined by $D(\mathbf{x}) = \nu$, where $D(\mathbf{x})$ is a continuous, three-dimensional function and ν is some constant [11]. Several authors have applied the MC approach to multiphase porous medium systems to obtain an approximate value of the amount of interfacial area between wetting and non-wetting phases. In general, this area cannot be obtained using the MC algorithm alone; and additional steps must be taken in order to estimate it. A common approach is to use a version of the MC algorithm to compute approximations to the locations of the interfaces bounding the solid, wetting, and non-wetting phases. Estimates of the desired interfacial area can be computed from these approximations [3, 4]. However, this approach cannot be used to compute other interfacial quantities, such as interfacial curvature, because the component interfaces are not constructed. Furthermore, the results of Dalla *et al.* [4] suggest that numerical estimates of interfacial areas obtained using this approach can have significant errors.

McClure *et al.* [12] described a modified marching cubes (MMC) algorithm designed to construct each of the component interfaces and the common curve present in two-fluid-phase porous medium systems. From these objects, interfacial areas and common curve lengths can be computed in a straightforward manner. The MMC approach has been shown to achieve accurate estimates of interfacial areas and common curve lengths for systems constructed analytically, and these approaches are directly applicable to results generated using the lattice-Boltzmann method [12]. In the present work, we demonstrate how the MMC approach may be used to obtain approximations of interfaces and common curves in experimental systems from data generated using CMT. The specific objectives of this work are: (1) to develop and assess procedures needed to apply the MMC algorithm to CMT data; (2) to use these procedures to approximate the interfaces and common curves in a multiphase porous medium system and to generate estimates of the measure of the extent of these entities; and (3) to estimate the mean curvature of an interface.

2. METHODS

In a three-phase porous media system, three interfaces $\Omega_{wn}, \Omega_{ws}, \Omega_{ns}$ and one common curve Ω_{wns} may exist. The objective of the MMC algorithm is to construct approximations of these objects from values of two continuous functions, $S(\mathbf{x})$ and $F(\mathbf{x})$, each of which is known at the node points of a regular grid. The interfaces in the system are obtained as isosurfaces from these functions, with $S(\mathbf{x}) = \nu_s$ corresponding to the solid surface, and $F(\mathbf{x}) = \nu_{wn}$ corresponding to the interface between wetting and non-wetting fluids. As in the MC algorithm, surface approximations are formed by marching through the cubes formed by adjacent grid nodes and constructing a list of triangles corresponding to the desired surface.

In the MMC algorithm, three possibilities exist for each grid cube in a three-phase system: (1) only one phase is present in the cube, (2) two phases are present in the cube, or (3) all three phases are present in the cube. For Case 1, no interfaces or common curves exist in the cube. For Case 2 one interface is present, but no common curve. For Case 3, three interfaces and a common curve exist. For a Case 2 cube, the steps used in the standard MC algorithm are applied to obtain the interface. For a Case 3 cube, the MC algorithm is used first to construct the solid surface; then interpolation is applied to approximate $F(\mathbf{x})$ on the solid surface. Linear interpolation along triangle legs may next be used to determine the location of points on the common curve $\check{\Omega}_{wns}$, where the hat has been used to denote that this object is an approximation. Subdivision of the solid surface at the common curve is used to obtain the interface approximations $\check{\Omega}_{ws}$ and $\check{\Omega}_{ns}$. Points on the wn interface are then determined along cube edges, excluding any points for which $S(\mathbf{x}) < \nu_s$. These points are combined with the common curve points to obtain the triangle vertices for the approximation $\check{\Omega}_{wn}$. Further details of the MMC algorithm may be found in McClure *et al.* [12].

To apply the MMC approach, we must first obtain suitable functions $F(\mathbf{x})$ and $S(\mathbf{x})$, along with isovalues ν_s and ν_{wn}. The general procedure that we use to obtain this information from CMT data is shown in Fig. 1. Unprocessed CMT data consists of initial and final energy intensities for a large number of photon beams that are passed through a sample at different angles. Inversion of this data yields a three-dimensional representation of the photon attenuation in each voxel

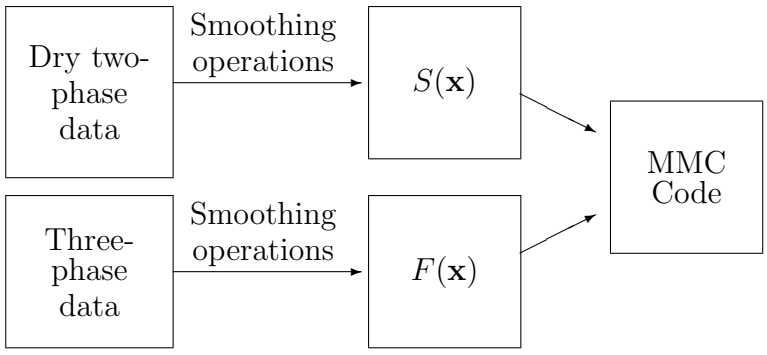

FIGURE 1. Formatting procedure used to obtain input data for the MMC approach from data obtained using x-ray tomography.

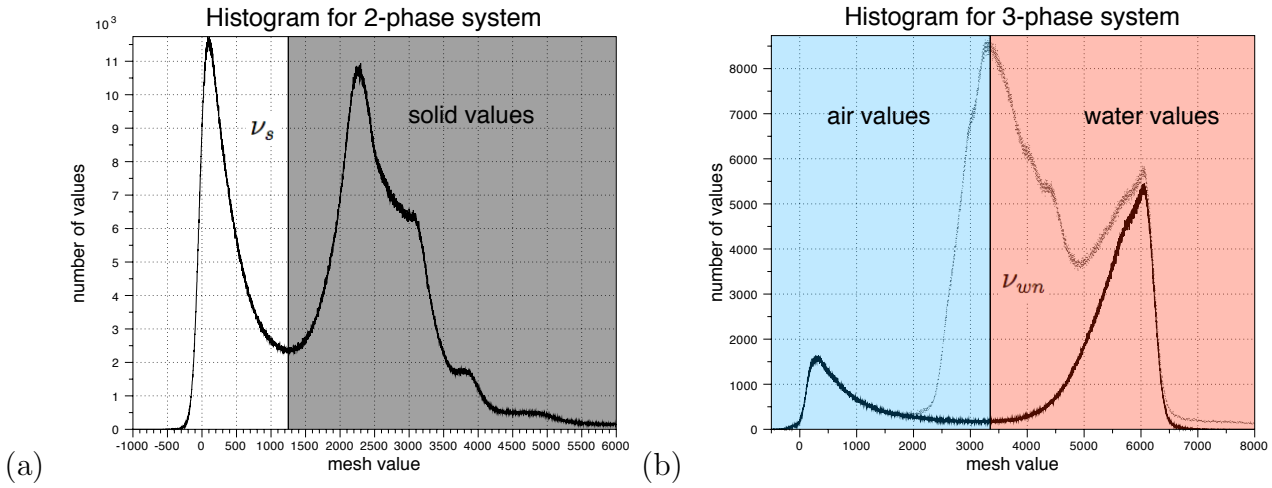

FIGURE 2. Histograms showing the range of mesh values occupied by: (a) two-phase and (b) three-phase data. Isovalues ν_s and ν_{wn} determine the range of values corresponding to each phase.

in the system. This information is passed to the formatting procedure outlined above in the form of a dry two-phase image obtained prior to the injection of any fluid into the system, and serves as the source of information for the function $S(\mathbf{x})$. Subsequently, three phase systems are analyzed and the photon attenuation distribution is used to compute $F(\mathbf{x})$.

Similarly to the MC algorithm, the MMC algorithm is designed to work most effectively when $F(\mathbf{x})$ and $S(\mathbf{x})$ are smooth functions. Typically, the initial images obtained using CMT are not sufficiently smooth to apply either of these approaches directly without significant error. Because of this, smoothing operations are applied to the data to reduce variations that occur due to experimental effects and noise in the reconstruction step. The most widely used smoothing operators are the mean filter, the median filter, and the Gaussian filter. The mean and Gaussian filters are discrete convolution operators, while the median filter selects the median value from a fixed number of neighboring values. In our approach, we apply a $3 \times 3 \times 3$ mean filter operation twice to obtain $S(\mathbf{x})$ and $F(\mathbf{x})$. More information about smoothing operators can be found in Davies [5]. For the systems under consideration here, this filtering provided sufficiently smooth fields, while still preserving sharp interfaces of interest.

Determination of the isovalues ν_s and ν_{wn} was accomplished using histograms as shown in Fig. 2. First, ν_s was assigned the value occurring the minimum number of times within the region separating the two peaks corresponding to the solid and void-space values. This selection minimizes the likelihood that regions within the pore-space would be misclassified as being inside the solid, or vice versa. For the fluid interface isovalue, ν_{wn}, three-phase data was used. For this data, three distinct peaks were observed corresponding to the values for each phase. Using information from the two-phase data, we cropped out the solid phase values to yield a histogram showing only air and water values, as shown in Fig. 2 (b). This isovalue ν_{wn} was chosen to be the maximum value of the solid phase, which was also near the value occurring

the minimum number of times in the region separating the two peaks in the cropped air-water histogram. This choice is logical because it minimizes the possibility that regions of wn interface will be mistakenly found near the solid.

After surface approximations were obtained using the MMC algorithm, these surfaces were used to compute other interfacial quantities. One such quantity is the mean curvature of the interface between wetting and non-wetting fluids, which is defined at the microscale as

$$J_{wn} = \nabla \cdot \mathbf{n}_{\boldsymbol{wn}} \tag{1}$$

where $\mathbf{n}_{\boldsymbol{wn}}$ is the unit normal to the wn surface. However, $F(\mathbf{x}) = \nu_{wn}$ at the interface so that this equation may be rewritten as [14]

$$J_{wn} = \nabla \cdot \frac{\nabla F}{|\nabla F|}. \tag{2}$$

Because the function $F(\mathbf{x})$ is defined in all of space, the mean curvature may be computed numerically at all grid points by evaluating eqn (2) using standard finite difference stencils to approximate the derivatives. An interpolation scheme was then applied to obtain approximate values of J_{wn} for all points on the approximate surface $\breve{\Omega}_{wn}$. The average mean curvature, J^{wn}, was computed by integrating J_{wn}over Ω_{wn}

$$J^{wn} = \frac{\int_{\Omega_{wn}} J_{wn}\, \mathrm{d}\mathfrak{r}}{\int_{\Omega_{wn}} \mathrm{d}\mathfrak{r}}. \tag{3}$$

3. RESULTS AND DISCUSSION

(a) (b)

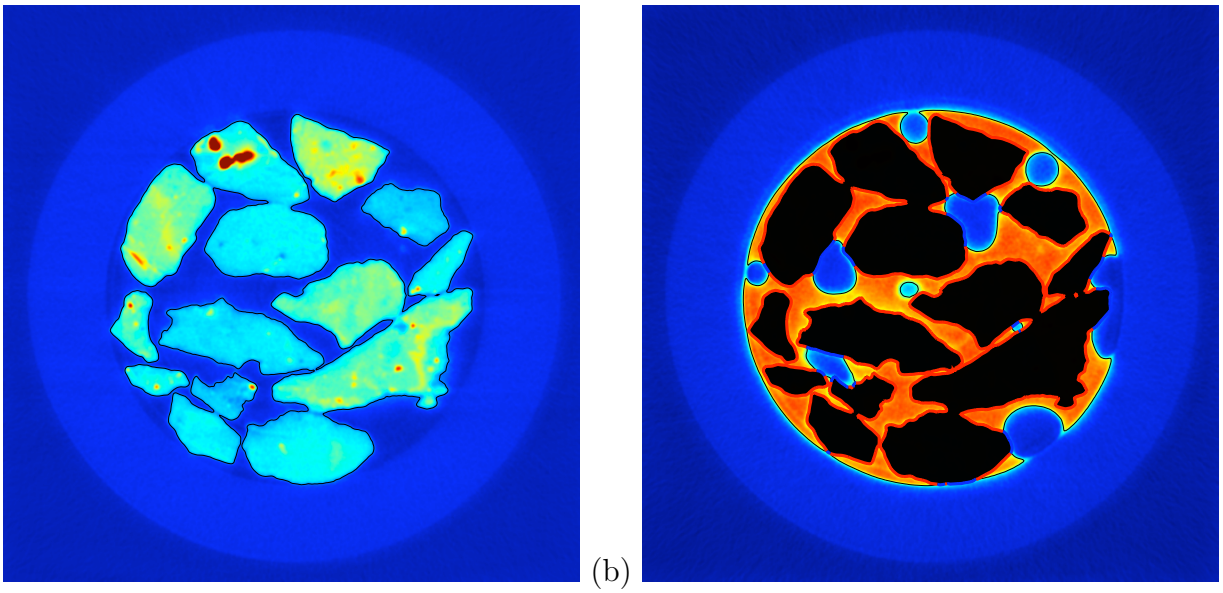

FIGURE 3. Slice of CMT data set showing (a) two- and (b) three-phase data along with approximations to $\breve{\Omega}_{wn}, \breve{\Omega}_{ws},$ and $\breve{\Omega}_{ns}$ constructed using MMC.

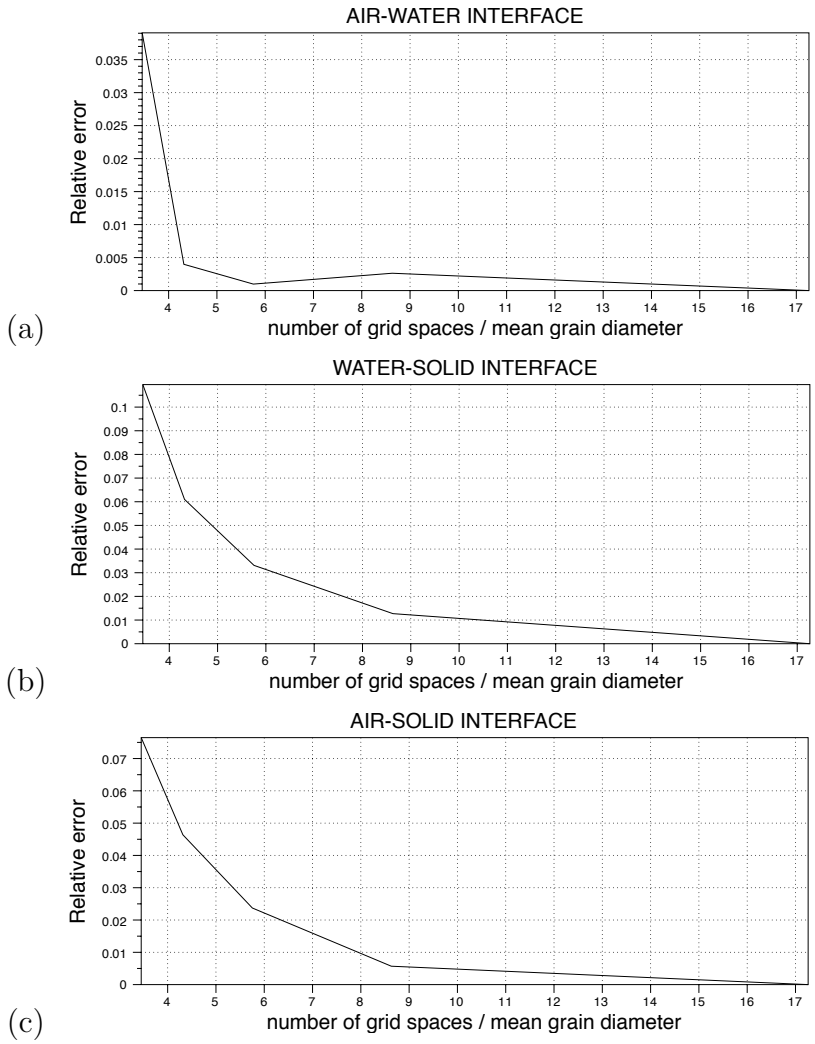

FIGURE 4. Relative error for interfacial areas computed from the MMC surfaces $\breve{\Omega}_{wn}, \breve{\Omega}_{ws}$ and $\breve{\Omega}_{ns}$. The number of voxels per mean grain diameter (0.58 mm) is plotted on the x-axis. The value of the interfacial area at the finest grid resolution was assumed to be exact.

We analyzed CMT data for an air-water-solid system by applying the formatting procedure shown in Fig. 1. The system was described by approximate values of the photon attenuation coefficient on a $650 \times 650 \times 280$ mesh with a constant grid spacing of 16.8 μm. The data set analyzed corresponded to to saturation conditions near the end of secondary imbibition. Consequently the capillary pressure for this system was close to zero. The air-water interfacial tension was 0.0681 N/m.

Interfacial areas for each of the component surfaces were computed using the interfaces obtained with the MMC algorithm. To assess the accuracy of the approach, we applied MMC to a subdomain of size $150 \times 150 \times 150$, using a series of meshes obtained by sparsifying this subdomain.

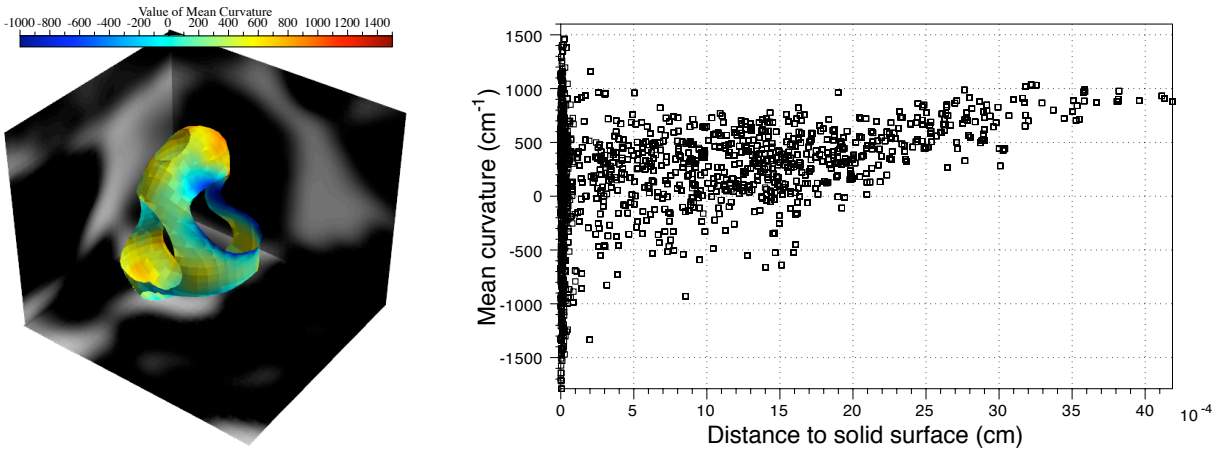

FIGURE 5. Curvature of the *wn* interface for a region of CMT data.

The interfacial area value obtained for the finest mesh was used to compute relative error for the interfacial area estimates obtained using the coarser meshes. Plots of this relative error are shown for each of the interfaces in Figs. 4 (a), (b), and (c). The grid spacing in this system is normalized with respect to the mean grain diameter, which was determined to be 0.58 mm using a sieve analysis.

The mean curvature of the *wn*-interface was evaluated using the computational approach outlined in the previous section. We found that the curvature varied significantly over the interface, both throughout the system and on individual interfaces. This variation was expected because of the existence of disconnected phases. The capillary pressure, which is the product of the interfacial tension and the mean curvature, of individual isolated non-wetting phase features was expected to vary as well. For individual interfaces, such as the one shown in Fig. 5, the presence of films coating the solid phase may also influence the curvature. As a consequence, the curvature of an individual interface, though expected to be constant based on Laplace's equation, may, in fact, vary with position on the interface. To illustrate this effect, we computed the distance to the solid surface for each location where a value of curvature was computed on $\check{\Omega}_{wn}$. These values are plotted in Fig. 5. From this figure, it can be observed that variability in the curvature is inversely related to the distance of a point on the interface from the closest solid surface. This observation is consistent with the idea that the geometry of the solid surface influences the curvature of the *wn* interface. We also found that the interfacial curvature approaches a constant value at greater distances from the solid surface. However, due to the presence of a disconnected phase, the relation between the macroscale capillary pressure and the interfacial curvature is complex.

4. CONCLUSIONS

An MMC approach was used to approximate the interfaces and common curves in a three-phase system visualized using CMT. Accurate estimates of interfacial areas were obtained. The mean

curvature for the air-water interface was also computed, and we observed significant variation in this curvature both for the full system and for individual interfaces. Computation of the distance to the solid surface for each point on the air-water interface showed that the variability in curvature is greater for parts of the interface closer to the solid surface. Future research will focus on developing a better understanding of the factors determining interfacial curvatures in multiphase porous medium systems and the use of interfacial quantities to advance the state of macroscale multiphase porous media models.

Acknowledgments

This work was supported in part by National Science Foundation grants DMS-0327896, EAR 0337711 and EAR-0337535, and by National Institute of Environmental Health Sciences grant P42 ES05948.

References

1. C. T. Chang, J. Qiao, S. Chen, and A. T. Watson, *Fracture characterization with nmr spectroscopy techniques*, Journal of Magn Resonance **126** (1997), 212–220.
2. K. A. Culligan, D. Wildenschild, B. S. B. Christensen, W. G. Gray, and M. L. Rivers, *Pore-scale characteristics of multiphase flow in porous media: A comparison of air-water and oil-water experiments*, Advances in Water Resources **29** (2006), no. 2, 227–238.
3. K. A. Culligan, D. Wildenschild, B. S. B. Christensen, W. G. Gray, M. L. Rivers, and A. F. B. Tompson, *Interfacial area measurements for unsaturated flow through a porous medium*, Water Resources Research **40** (2004), no. 12.
4. E. Dalla, M. Hilpert, and C. T. Miller, *Computation of the interfacial area for two-fluid porous medium systems*, Journal of Contaminant Hydrology **56** (2002), no. 1-2, 25–48.
5. E. Davies, *Machine vision: theory, algorithms, practicalities*, Academic Press, San Diego, 1997.
6. W. G. Gray and S. M. Hassanizadeh, *Macroscale continuum mechanics for multiphase porous-media flow including phases, interfaces, common lines and common points*, Advances in Water Resources **21** (1998), no. 4, 261–281.
7. S. M. Hassanizadeh and W. G. Gray, *Thermodynamic basis of capillary-pressure in porous-media*, Water Resources Research **29** (1993), no. 10, 3389–3405.
8. R. J. Held and M. A. Celia, *Modeling support of functional relationships between capillary pressure, saturation, interfacial area and common lines*, Advances in Water Resources **24** (2001), no. 3-4, 325–343.
9. M. L. Johns and L. F. Gladden, *Magnetic resonance imaging study of the dissolution kinetics of octanol in porous media*, Journal of Colloid and Interface Science **210** (1999), no. 2, 261–270.
10. H. N. Li, C. X. Pan, and C. T. Miller, *Pore-scale investigation of viscous coupling effects for two-phase flow in porous media*, Physical Review E **72** (2005), no. 2.
11. W. E. Lorenson and H. E. Cline, *Marching cubes: a high resolution 3D surface construction algorithm*, Computer Graphics **21** (1987), no. 4.

12. J. E. McClure, D. Adalsteinsson, C. Pan, C. T. Miller, and W. G. Gray, *Approximation of interfacial properties in porous medium systems*, in press, Advances in Water Resources (2006).
13. P. C. Reeves and M. A. Celia, *A functional relationship between capillary pressure, saturation, and interfacial area as revealed by a pore-scale network model*, Water Resources Research **32** (1996), no. 8, 2345–2358.
14. J. A. Sethian, *Level set methods and fast marching methods: evolving interfaces in computational geometry, fluid mechanics, computer vision, and materials science*, Cambridge University Press, New York, 1999.
15. D. Wildenschild, J. W. Hopmans, C. M. P. Vaz, M. L. Rivers, D. Rikard, and B. S. B. Christensen, *Using x-ray computed tomography in hydrology: systems, resolutions, and limitations*, Journal of Hydrology **267** (2002), no. 3-4, 285–297.